Int J Adv Manuf Technol (2017) 93:4345–4356
DOI 10.1007/s00170-017-0871-3

ORIGINAL ARTICLE

Multiobjective optimization of processing parameters in longitudinal-torsion ultrasonic assisted milling of Ti-6Al-4V

Ying Niu [1] · Feng Jiao [1] · Bo Zhao [1] · Dong Wang [1]

Received: 28 April 2017 / Accepted: 24 July 2017 / Published online: 7 August 2017

Abstract In order to solve the problems of high cost and low efficiency in milling of titanium alloy, multiobjective optimizations are proposed to optimize machining and ultrasonic parameters by nondominated sorting genetic algorithm II (NSGA-II). In the present work, longitudinal-torsion ultrasonic vibration has been superimposed to the milling of titanium alloy (Ti-6Al-4V). Orthogonal experiment of milling has been carried out to evaluate influence of the parameters on machining results. Then, to meet the different engineering demands, three multiobjective optimization models are established to obtain optimization parameters. According to the optimization results, a group of milling verified experiments was developed for optimized models. The results show that the three optimization models balance the different objective well, and the optimization results are close to experiment results. It provides choices for engineering application.

Keywords Ti-6Al-4V · Longitudinal-torsion ultrasonic vibration · Multiobjective optimization · NSGA-II

1 Introduction

Titanium alloy has a series of excellent properties such as corrosion resistance, high strength, and good heat resistance [1–3], widely used in medical treatment, aerospace, and other fields. It is considered as a typical difficult-to-machine material, due to its chemical, physical, and mechanical properties, for instance cutting temperature is high, friction force is large, tool wear is serious, and so on [4–6]. So it is very meaningful to improve the processing efficiency and quality.

A large number of studies have shown that ultrasonic vibration cutting is an effective machining method for difficult-to-machine material [7, 8]. Ko et al. [9] found that it was helpful to improve the surface quality and stress, while appropriate feed per tooth was adopted in ultrasonic vibration milling. Ahmed et al. [10] developed rotary ultrasonic system in milling of alumina, and lower cutting force and better surface quality were obtained. Hara et al. [11] performed ultrasonic vibration in the cutting of steel. The periodic rippling was formed on machined surface. While low amplitude and high cutting speed were adopted, the result was similar to low speed cutting. Wang et al. [12] studied the influence of machining parameters on the surface quality in ultrasonic torsional vibration milling of titanium alloy. It proved that it could reduce obviously the surface roughness in ultrasonic torsional milling, and large amplitude and low milling speed are more conducive to reduce surface roughness (SR). Jiang et al. [13] developed an elliptic ultrasonic in milling of titanium alloy. Cutting force can be reduced to 50%. Soutome et al. [14] analyzed surface quality in high-speed cutting of alumina. The better SR could be obtained while proper direction of vibration was adopted.

Great attention has been paid to the optimization of machining process in recent years, and a lot of researches have been done from different angles, such as tool inclination angle, tool path, cutting parameters, and so on. Among them, the optimization of cutting parameters plays a decisive role in the tool durability, processing stability, and workpiece quality. Budak et al. [15], based on the theory of chatter, studied the selection method of axial depth of cut and radial depth of cut, to achieve the maximum material removal rate. Merdol et al. [16] considered the constraints of cutting force, chip thickness, spindle power, workpiece dimension error, and

✉ Feng Jiao
jiaofeng@hpu.edu.cn

[1] School of Mechanical and Power Engineering, Henan Polytechnic University, Henan, China

Table 1 Main chemical composition of Ti-6Al-4V

Element	Ti	Al	V	Fe	O	C	H	N
Wt (%)	matrix	5.5–6.8	3.5–4.5	0.3	0.2	0.1	0.015	0.05

machining stability, and a general optimization strategy of cutting parameters was proposed. Liu et al. [17] optimized and predicted of surface roughness by particle swarm optimization. Mahdavinejad et al. [18] presented a method of multi-perceptron artificial neural network to optimization of cutting parameters, and better surface roughness was obtained. Brecher et al. [19] pointed out the problem of poor surface quality in machining, main caused by the inter-action effect of machine tools and cutting process.

From the analysis of cutting optimization, in view of the complexity of machining process of titanium alloy, several different and even conflicting goals need to be met as much as possible, so multiobjective optimization of cutting parameters has more application value. Experiment method is intuitive and easy to realize, however, due to restrictions on the number of data is discrete and cannot describe the chance of dynamically output with the cutting parameters. It realizes optimization by mathematical model, but it only fits for the single-objective optimization requirement. In contrast, genetic algorithm, particle swarm optimization, and other evolutionary algorithms can search the solution space in parallel and have a good ability to find the optimal or suboptimal solution. It is suitable for solving multiobjective optimization problems. Li et al. [20], Chakraborti et al. [21], Koura et al. [22], and Gholami et al. [23] established the multiobjective optimization model using nondominated sorting genetic algorithm II (NSGA-II), respectively, and verified the optimization results, and the results showed that NSGA can effectively solve the problems of multiobjective optimization.

In the present work, longitudinal-torsion ultrasonic vibration has been superimposed to the milling of titanium alloy (Ti-6Al-4V). Based on the orthogonal experiment design, milling experiments have been proposed to evaluate the influence of the machining and ultrasonic parameters on

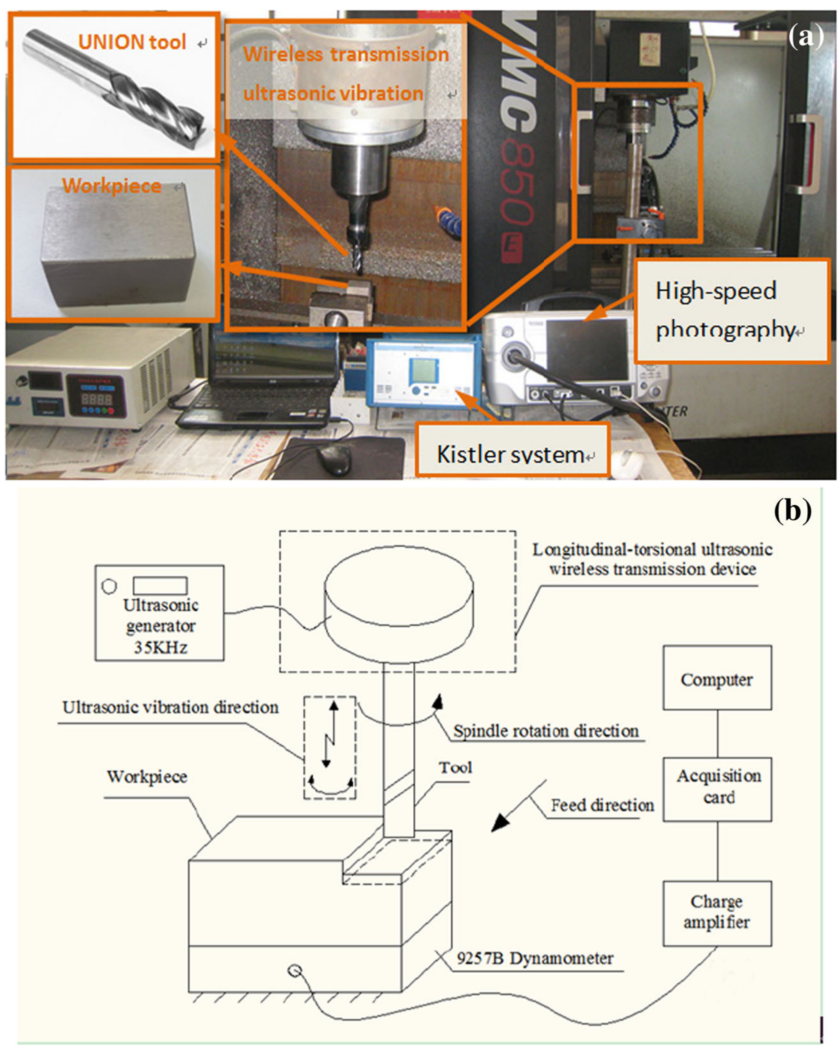

Fig. 1 **a**, **b** The experimental devices

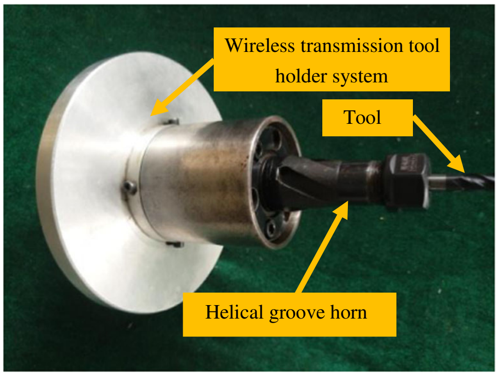

Fig. 2 The horn with helical groove

machining results. The empirical models of residual stress (*RS*), *SR*, and surface hardness (*SH*) have been developed through logarithmic model. Then, to meet the different demands, three multiobjective optimization models are established to optimize milling parameters. Multiobjective optimization I aims to coupling optimize of the material removal rate (*MRR*) and surface quality RS. The multiobjective objective II aims to coupling optimize of the processing efficiency MRR and SR. Meanwhile, multiobjective optimization III aims to coupling optimize of SR and SH. Finally, a group of milling verified experiments was carried out for optimized results.

2 Experiment setup and design

In this work, a series of longitudinal-torsion ultrasonic vibration assisted milling of Ti-6Al-4V experiments have been proposed, RS, SR, and SH were measured. According to the experimental results, influence of the machining and amplitude of ultrasonic parameters on machining quality have been analyzed, and then the empirical models of RS, SR, and SH have been developed through regression analysis.

2.1 Experiment setup

The end milling experiments were carried out on vertical machining center VMC-850E. As the workpiece material, chemical composition of Ti-6Al-4V was listed in Table 1, and the size of rectangular workpiece was 30 mm × 20 mm × 20 mm. The experimental equipment was composed of Kistler dynamometer system (9257B), self-developed wireless transmission longitudinal-torsion ultrasonic vibration assisted milling system (the amplitude ratio of longitudinal and torsion was 1:1; detail in Section 2.2), high-speed photography, and computer. In machining processing, the cemented carbide UNION tool (C-CES 10*25) was adopted. The experimental devices and machining schematic are shown in Fig. 1a, b.

2.2 Self-developed wireless transmission longitudinal-torsion ultrasonic vibration systems

The realization of longitudinal-torsional vibration mainly depends on helical groove horn, as in Fig. 2, single-excited longitudinal vibration is converted to longitudinal-torsional vibration through the helical groove, the frequency is about 35 kHz, and the amplitude could be adjusted from 2 to 6 μm by changing the power of generator and elongation of milling tool. From simulation models in Fig. 3, the longitudinal-torsional vibration is visible at the output end. Then, the simulation of frequency is verified by impedance tests in Fig. 4.

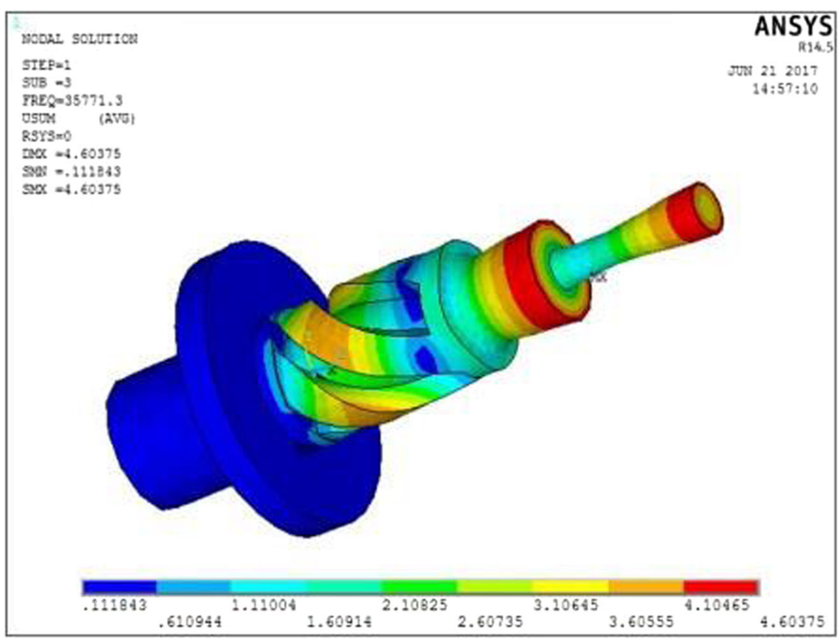

Fig. 3 Simulation of vibration frequency and modes

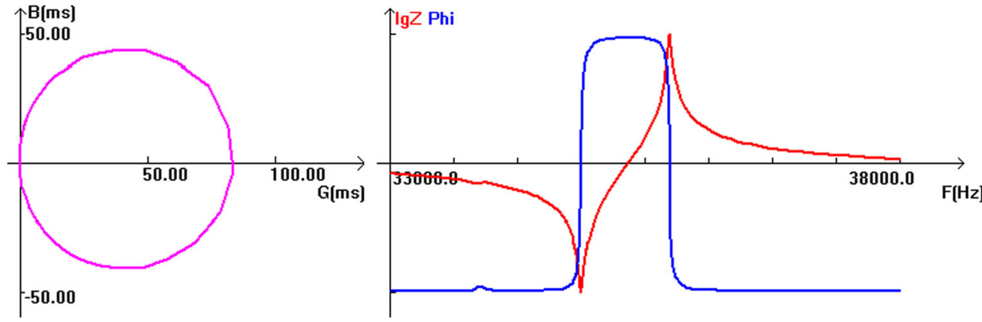

Fig. 4 Impedance test of helical groove horn

The amplitude of longitudinal can be measured directly through infrared displacement sensor; however, it is difficult to measure the amplitude of torsional directly, and a novel measurement method was found as follows. The milling tool was prefabricated in a small plane in the radial direction and the amplitude of torsional is calculated by measuring result of radial amplitude. It is illustrated in Fig. 5. Line-segment AC is the radial amplitude of point A measured by infrared displacement sensor, R is the radius of tool (R = 5 mm), AE can be measured directly, and ED is the amplitude of torsional. It can be solved by Eqs. (1) to (3).

It is found that the amplitude ratio between longitudinal and torsional is about 1:1, through repeated-measure, as shown in Fig. 6. Therefore, the expressed amplitude of vibration represents the amplitude of longitudinal and torsional.

$$AO = R - EA \tag{1}$$

$$\theta = \arctan\frac{AC}{AO} \tag{2}$$

$$ED = {}^{\theta \times \pi \times R}/_{180} \tag{3}$$

2.3 Experiment design

The orthogonal experiment method was adopted with five parameters and with five levels. The parameters included milling speed (*MS*), feed per tooth (*FpT*), width of cut (*WoC*), depth of cut (*DoC*), and amplitude of ultrasonic (*AoU*), and it is listed in Table 2.

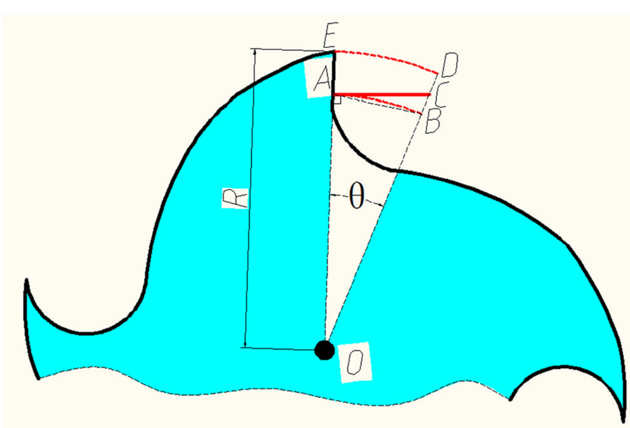

Fig. 5 Illustrative diagram of torsional amplitude measured

3 Experimental results and discussion

After milling experiments, RS was measured with the help of the PROTO X-ray by using XRD method, and Cu target has been chosen. The measurement method of residual stress was presented in Fig. 7. The residual stress in feed direction is used to evaluate the physical property of machined quality. The average of two measurements results is taken as the results.

The surface roughness Ra is measured in feed direction by Taylor Hobson roughometer (Surtronic 3+). The average value of four measuring results is used to evaluate surface roughness.

Surface hardness is measured by a micro-hardness instrument (MH-5). The average value of two measuring is used to evaluate surface hardness, as shown in Fig. 8, where test force is 50 N and retention time is 5 s.

The experimental results are showed in Table 3, while *MRR* was obtained by calculation from Eq. (4), where, v, z, f_z, a_p, a_e, d is MS, number of teeth, FpT, DoC, WoC, and tool diameter (φ10 mm), respectively.

$$MRR = \frac{1000v}{\pi d} \times z \times f_z \times a_p \times a_e \tag{4}$$

From Table 3, all SR are negative. As indicated, residual compressive stress (*RCS*) can be obtained under all selected processing parameters in this work, which proved that longitudinal-torsion ultrasonic vibration assisted milling is an effective anti-fatigue machining method for milling of Ti-6Al-4V. Meanwhile, the better SR and SH are obtained as well.

3.1 Results and discussion of residual stress

Figure 9 was drawn according to the experimental results of RS from Table 3. Then, the effects of parameters on RS are analyzed. It can be seen from Fig. 9 that the RCS can be obtained in all the selected parameters, especially, and a large RCS can be obtained by small machining parameters and

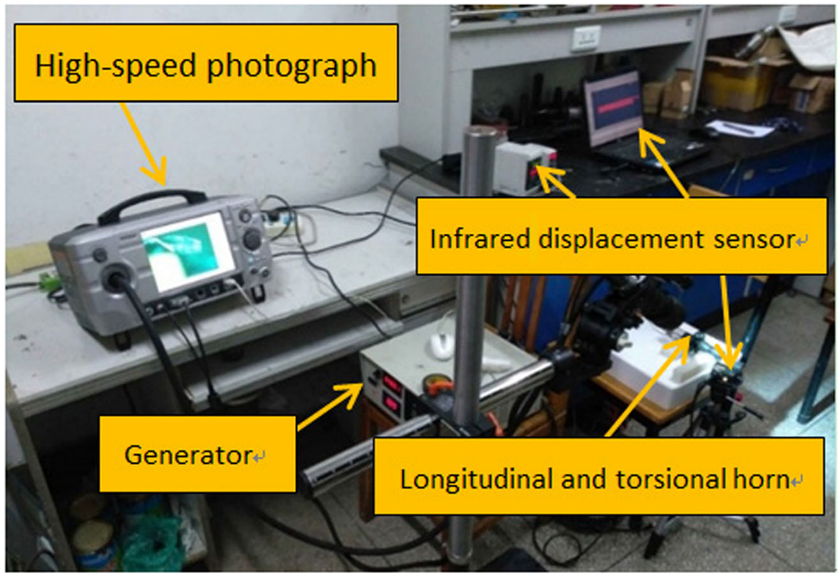

Fig. 6 The amplitude measuring device

appropriate amplitude. Specifically, the RCS decreases first and then fluctuates with the increase of all machining parameters. On the one hand, the separation characteristics of ultrasonic become feebler with the increase of MS and FPT. It weakens the effect of ultrasonic surface strengthening. On the other hand, the cutting heat and cutting force increase with the increase in MRR. It reduces the RCS, and with cutting parameters, it continues to increase. Partly, the material removal mode changes from shearing to squeezed. It helps improve RCS. Meanwhile, the RS appears fluctuating with an increase of amplitude. Therefore, it is very important to choose the appropriate parameters to obtain the different RCS.

According to experimental results, the RS model was established from Eq. 5 to Eq. 8.

$$f_1 = \sigma = -c_0 v^{c_1} f_z^{c_2} a_e^{c_3} a_p^{c_4} A^{c_5} \quad (5)$$

$$\lg|\sigma| = \lg c_0 + c_1 \lg v + c_2 \lg f_z + c_3 \lg a_e + c_4 \lg a_p + c_5 \lg A \quad (6)$$

$$\lg|\sigma| = 2.763 - 0.3439 \lg v - 0.2020 \lg f_z - 0.2635 \lg a_e - 0.0919 \lg a_p + 0.0520 \lg A \quad (7)$$

Table 2 Parameters and levels

Levels	MS v, m/min	FpT f_z, mm/z	WoC a_e, mm	DoC a_p, mm	AoU A, μm
1	20	0.01	1	0.15	2
2	40	0.018	2	0.3	3
3	60	0.026	3	0.45	4
4	80	0.034	4	0.6	5
5	100	0.042	5	0.75	6

$$f_1 = \sigma = -549.4 v^{-0.3439} f_z^{-0.2020} a_e^{-0.2635} a_p^{-0.0919} A^{0.0520} \quad (8)$$

In order to directly reflect the influence of processing parameters on the result, the sensitivity of processing parameters on RS was obtained in Fig. 10. It can been seen that MS has the greatest influence on the RS. Contribution rate reaches 36.07%. WoC, FpT, and DoC followed is 27.64, 21.19, and 9.64%, respectively. The reason is that the parameters have great influence on cutting force and cutting temperature, the effect of thermal-force has a great influence on the RS. The influence of AoU is 14.43%, ultrasonic vibration reduces cutting heat effectively, and moreover, it provides impact force on surface, both of them improve RCS, however, amplitude has a smaller influence on the RS.

3.2 Results and discussion of surface roughness

The influence of parameters on Ra from Table 3 was presented in Fig. 11. It can be seen that better Ra can be obtained in all the selected parameters, specifically: Ra rising on a whole with the increase of FpT and DoC. The reason is that residual peak between the two teeth increases with the increase in FpT and DoC. The possibility of machining defects increases as well. From the mechanism of ultrasonic assisted milling, it could reduce the height of the residual peak, and the peak increases with the increase of amplitude. The MRR increased with the WoC increased and caused surface cracks, microhole, and other defects. It reduces the surface quality; however, Ra is improved when WoC is 5 mm. It is possible to reduce friction between the flank and the machined surface. Therefore, it is very important to choose the appropriate parameters to obtain the better Ra.

According to experimental results, the Ra model was established from Eq. 9 to Eq. 12.

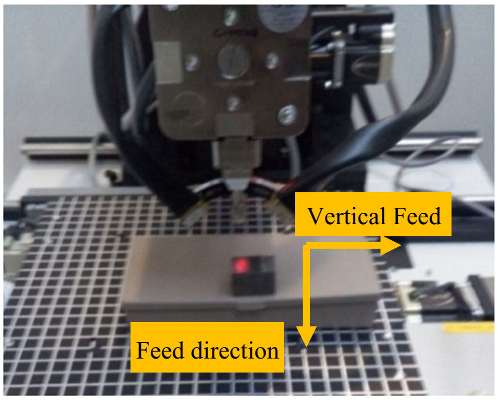

Fig. 7 Residual stress measurement

$$\mathrm{Ra} = c_0 v^{c_1} f_z^{c_2} a_e^{c_3} a_p^{c_4} A^{c_5} \tag{9}$$

$$\mathrm{lgRa} = \mathrm{lgc}_0 + c_1 \mathrm{lg}v + c_2 \mathrm{lg}f_z + c_3 \mathrm{lg}a_e + c_4 \mathrm{lg}a_p + c_5 \mathrm{lg}A \tag{10}$$

$$\mathrm{lgRa} = 0.1887 + 0.0125\mathrm{lg}v + 0.2756\mathrm{lg}f_z + 0.0981\mathrm{lg}a_e + 0.1078\mathrm{lg}a_p + 0.1517\mathrm{lg}A \tag{11}$$

$$f_2 = Ra = 1.544v^{0.0125} f_z^{0.2756} a_e^{0.0984} a_p^{0.1078} A^{0.1517} \tag{12}$$

The sensitivity of processing parameters on Ra was obtained in Fig. 12. From the figure, FpT has a greatest influence on the Ra. AoU followed, and both contribution rates reach 66.14%. DoC and WoC have similar effects on the Ra, 16.69% and 15.23%, respectively. MS has a smallest influence on Ra, only 1.93%.

3.3 Results and discussion of surface hardness

According to the experimental results of SH, Fig. 13 was presented, and then effects of parameters on SH are analyzed. It is shown that SH rise on a whole with the increase of AoU, the impact energy of the tool on the workpiece increases with the increase of AoU, and it increases surface hardness. And the curve of SH appears fluctuating with increase of other machining parameters. Thus, to obtain different SH, the appropriate parameters should be chosen. According to experimental results, the SH model was established from Eq. 13 to Eq. 16.

$$\mathrm{HV} = c_0 v^{c_1} f_z^{c_2} a_e^{c_3} a_p^{c_4} A^{c_5} \tag{13}$$

$$\mathrm{lgHV} = \mathrm{lgc}_0 + c_1 \mathrm{lg}v + c_2 \mathrm{lg}f_z + c_3 \mathrm{lg}a_e + c_4 \mathrm{lg}a_p + c_5 \mathrm{lg}A \tag{14}$$

$$\mathrm{lg}HV = 2.5421 + 0.0350\mathrm{lg}v + 0.0868\mathrm{lg}f_z + 0.0822\mathrm{lg}a_e + 0.0269\mathrm{lg}a_p + 0.2787\mathrm{lg}A \tag{15}$$

$$f_3 = HV = 348.4v^{0.035} f_z^{0.0868} a_e^{0.0822} a_p^{0.0269} A^{0.2787} \tag{16}$$

The sensitivity of processing parameters on Ra was obtained in Fig. 14. According to Eq. (16), as shown, AoU has the greatest influence on the SH. The contribution rate is more than half, and FpT and WoC are followed, 17.03 and 16.13%, respectively. Then, MS and DoC are 6.87 and 5.28%, respectively.

Based on the above analysis of the influence of processing parameters on the experimental results, it was found that the same factors have different effects on different response. Therefore, to meet the different engineering demands, appropriate parameters should be adopted, and it is necessary to establish multiobjective optimization models, especially in conflicting requirements.

3.4 Verification for empirical model

According to empirical model (Eqs. 8, 12, and 16) of RS, SR, and SH, predicted value would be calculated and then compared with the experimental results, as shown in Fig. 15. It

Fig. 8 Surface hardness measurement

Table 3 Design of experiments and results

No.	MS v, m/min	FpT f_z, mm/z	WoC a_e, mm	DoC a_p, mm	AoU A, μm	RS σ, MPa	SR Ra μm	SH H, HV	MRR Q, mm^3/min
1	20	0.01	1	0.15	2	−498.36	0.31	310.1	3.820
2	20	0.018	2	0.3	3	−443.47	0.89	349.9	27.503
3	20	0.026	3	0.45	4	−423.94	0.67	393.8	89.384
4	20	0.034	4	0.6	5	−259	0.89	594.6	207.799
5	20	0.042	5	0.75	6	−409.44	0.96	491.2	401.082
6	40	0.01	2	0.45	5	−351	1.06	599.4	45.838
7	40	0.018	3	0.6	6	−352.5	0.55	443.4	165.017
8	40	0.026	4	0.75	2	−266.67	1.07	410.7	397.262
9	40	0.034	5	0.15	3	−375	0.74	489.1	129.874
10	40	0.042	1	0.3	4	−399	0.72	364.8	64.173
11	60	0.01	3	0.75	3	−318.5	0.76	326	171.892
12	60	0.018	4	0.15	4	−397.36	0.74	344.6	82.508
13	60	0.026	5	0.3	5	−101	0.84	546.4	297.947
14	60	0.034	1	0.45	6	−320	0.47	523.1	116.887
15	60	0.042	2	0.6	2	−287	0.55	471.1	385.039
16	80	0.01	4	0.3	6	−233	0.70	494.3	122.235
17	80	0.018	5	0.45	2	−163	0.41	430.7	412.542
18	80	0.026	1	0.6	3	−330	0.70	347.5	158.905
19	80	0.034	2	0.75	4	−142.22	0.99	460.9	519.497
20	80	0.042	3	0.15	5	−255.44	0.86	568.5	192.519
21	100	0.01	5	0.6	4	−354.1	0.45	447.8	381.983
22	100	0.018	1	0.75	5	−378.5	0.63	483.2	171.892
23	100	0.026	2	0.15	6	−298	0.87	491.3	99.316
24	100	0.034	3	0.3	2	−227	0.92	371.2	389.623
25	100	0.042	4	0.45	3	−140.5	1.10	419.9	962.597

illustrates that prediction value is close to experimental results; thus, the model has a high prediction precision in the scope of the experiment.

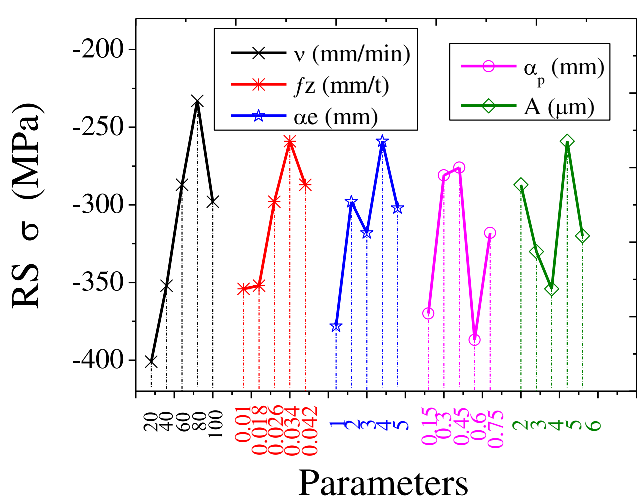

Fig. 9 Parameters' influence on RS

4 Multiobjective optimization results

Among the many multiobjective optimization methods, NSGA-II has features of fast nondominated sorting approach, fast crowded distance estimation procedure, and simple crowded comparison operator, so it is widely used in machining process [24, 25].

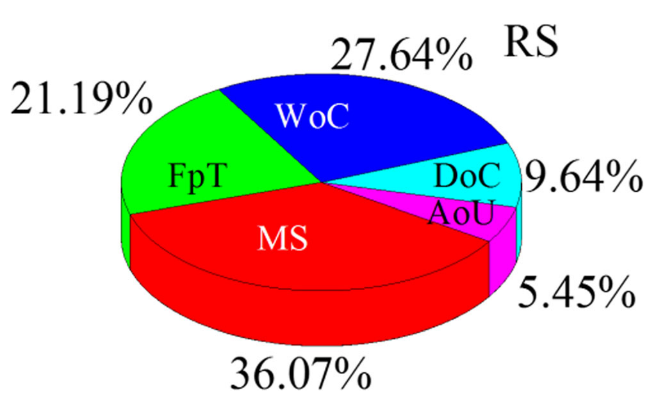

Fig. 10 The sensitivity of processing parameters on RS

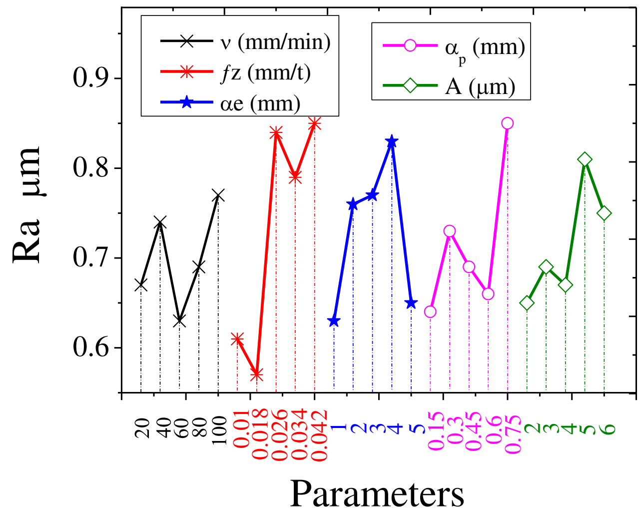

Fig. 11 Parameters' influence on Ra

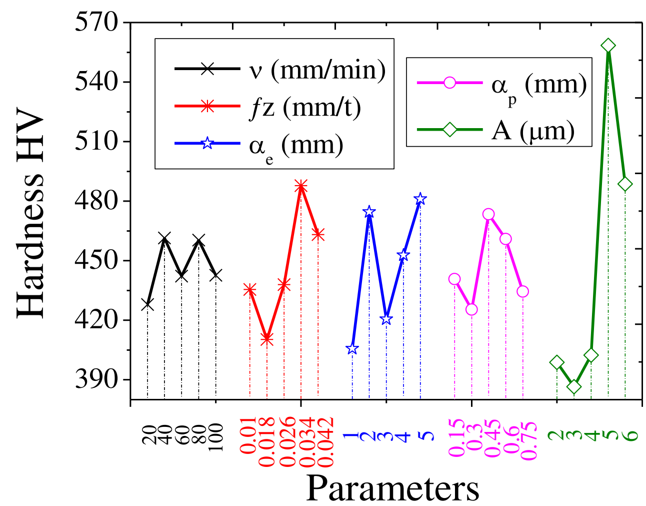

Fig. 13 Parameters' influence on SH

4.1 Constraint condition

The mathematical equations and constraint conditions of optimization procedure were established in the following sections.

First of all, construct optimization variables: x = (×1, ×2, ×3, ×4, ×5), ×1, ×2, ×3, ×4, ×5 representing the value of MS, FpT, WoC, DoC, and AoU.

Then, according to NSGA-II and experimental design, constraint conditions were constructed, as shown in Eqs. 17 to 21.

MS $20 \le V \le 100$:

$$\begin{cases} g_1(x) = 20 - x_1 \le 0 \\ g_2(x) = x_1 - 100 \le 0 \end{cases} \quad (17)$$

FpT $0.01 \le f_z \le 0.042$:

$$\begin{cases} g_3(x) = 0.01 - x_2 \le 0 \\ g_4(x) = x_2 - 0.042 \le 0 \end{cases} \quad (18)$$

WoC $1 \le a_e \le 5$:

$$\begin{cases} g_5(x) = 1 - x_3 \le 0 \\ g_6(x) = x_3 - 5 \le 0 \end{cases} \quad (19)$$

DoC $20 \le a_p \le 100$:

$$\begin{cases} g_7(x) = 0.15 - x_4 \le 0 \\ g_8(x) = x_4 - 0.75 \le 0 \end{cases} \quad (20)$$

AoU $2 \le A \le 6$:

$$\begin{cases} g_9(x) = 2 - x_5 \le 0 \\ g_{10}(x) = x_5 - 6 \le 0 \end{cases} \quad (21)$$

4.2 Multiobjective optimization results and discussion

Better surface quality and higher MRR are chased in the finishing machining process. However, it is focused on

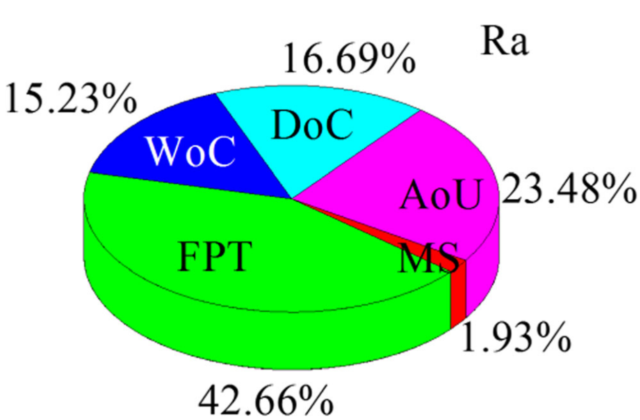

Fig. 12 The sensitivity of processing parameters on Ra

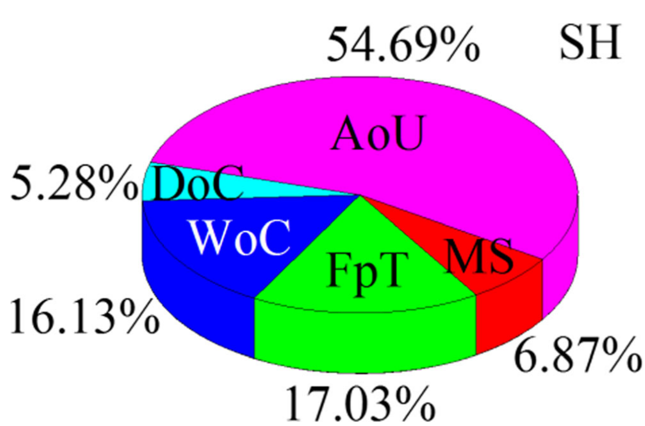

Fig. 14 The sensitivity of processing parameters on SH

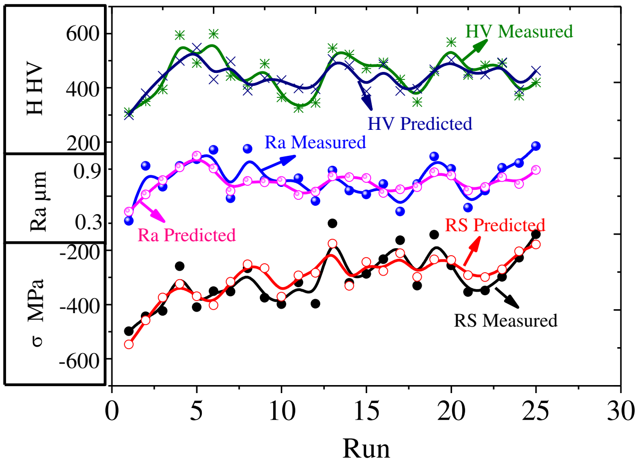

Fig. 15 Experimental vs. predicted value

different places in different applications. To meet the different demands, the present study established three different multiobjective optimization models to optimize processing parameters (including mill and AoU parameters). Multiobjective optimization I aims to coupling optimize of the processing efficiency MRR and surface quality RS. The multiobjective objective II aims to coupling optimize of the processing efficiency MRR and SR. Meanwhile, multiobjective optimization III aims to coupling optimize of SR and SH. In the optimization procedure, a population size of 200 and an evolutional generation of 100 were adopted.

4.2.1 Multiobjective optimization I

In order to obtain the anti-fatigue parts, an increase in the RCS on the machined surface is an effective method, while processing efficiency also needs to be considered. Thus, the multiobjective objective I considers optimization of MRR and RS simultaneously. The optimization model function is given in Eq. 22.

Table 4 Pareto optimal solutions for optimization I

MS v, m/min	FpT f_z, mm/z	WoC a_e, mm	DoC a_p, mm	AoC A, µm	RS σ, MPa	MRR Q, mm^3/min
21.5	0.036	1.50	0.73	6	−400	108.4
21.5	0.042	1.51	0.73	6	−387.9	126.6
24.4	0.036	1.87	0.69	6	−363.8	144.8
27.6	0.026	2.22	0.73	6	−354.6	147.8
22.0	0.037	2.87	0.70	6	−334	209.9
22.3	0.034	3.40	0.71	6	−323.3	233.1
27.1	0.027	3.49	0.74	6	−314.3	238.5
23.7	0.033	4.08	0.61	6	−307.5	249.9
21.9	0.036	4.53	0.71	6	−298.8	321.2
31.6	0.036	4.61	0.70	6	−262	468.5
30.7	0.040	4.52	0.71	6	−260.6	496
33.7	0.039	4.74	0.74	6	−248.8	589.7
37.5	0.039	4.65	0.74	6	−241.2	640.6

$$\begin{cases} Object: \min f(f_1(x), f_4(x)) \\ Find: x_1, x_2, x_3, x_4, x_5 \\ s.t.\ \ g_i(x) \le 0 \ \ i = 1, \cdots, 10. \end{cases} \tag{22}$$

After calculation, the Pareto front of optimization objective I is shown in Fig. 16.

From Fig. 16, the value of RCS decreases rapidly along with a litle increase of MRR in region A. Meanwhile, the MRR increases rapidly along with a litter decrease of RCS in region C. However, an inflection point appears in region B, that is to say, it balances the RCS and MRR in this region. Therefore, it is regarded as an optimal region to get bigger RCS and higher MRR. Some Pareto optimal solutions of region B are listed in Table 4.

From Table 4, to balance Min (RS) and Max (MRR), smaller MS (21.5–37.5 m/min), larger FpT (0.026–0.042 mm/z), and DoC (0.61–0.94 mm) should be considered. The reason is

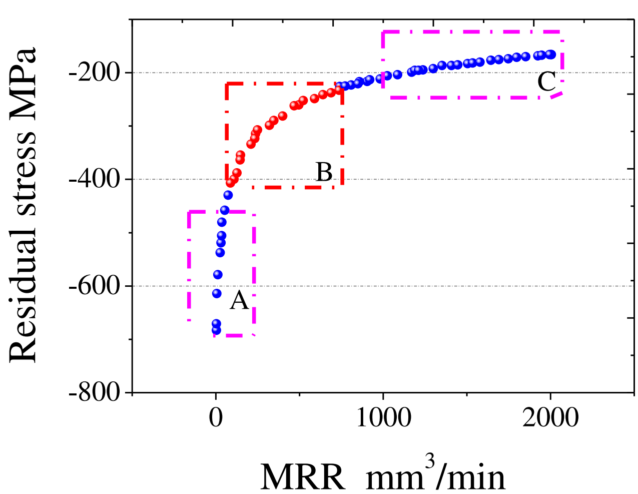

Fig. 16 Pareto front for multiobjective optimization I

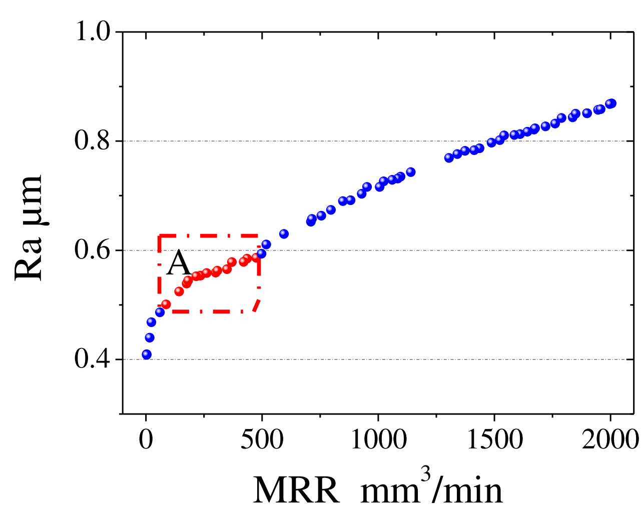

Fig. 17 Pareto front for multiobjective optimization II

Table 5 Some Pareto optimal solutions for optimization II

MS v, m/min	FpT f_z, mm/z	WoC a_e mm	DoC a_p mm	AoU A, μm	MRR Q, mm^3/min	SR Ra, μm
93.8	0.011	2.84	0.46	2	175.9	0.54
93.8	0.012	2.84	0.46	2	182.5	0.54
98.0	0.012	2.32	0.65	2	216.9	0.55
96.2	0.011	3.61	0.48	2	235.1	0.55
98.4	0.011	3.72	0.51	2	261.7	0.56
97.2	0.010	3.79	0.63	2	301.1	0.56
97.2	0.010	3.79	0.63	2	308.3	0.56
99.9	0.010	4.67	0.59	2	349.2	0.57
96.9	0.011	4.47	0.61	2	370.5	0.58
98.3	0.010	4.79	0.68	2	421.2	0.58
98.3	0.011	4.79	0.68	2	436.2	0.58
100.0	0.010	4.95	0.74	2	475.3	0.59
100.0	0.011	4.95	0.74	2	498.3	0.59

Table 6 Some Pareto optimal solutions for optimization III

MS v, m/min	FpT f_z, mm/z	WoC a_e, mm	DoC a_p, mm	AoU A, μm	SH H, HV	SR Ra, μm
86.8	0.011	1.04	0.15	2	329.6	0.43
86.8	0.010	1.02	0.15	3	337.5	0.43
86.8	0.011	1.02	0.15	3	338.3	0.44
87.0	0.010	1.03	0.15	3	343.7	0.44
86.9	0.010	1.03	0.15	3	351.7	0.44
86.9	0.011	1.03	0.15	3	353.7	0.45
86.9	0.010	1.02	0.15	3	361.1	0.45
88.3	0.010	1.05	0.16	3	368.9	0.46
86.8	0.010	1.03	0.15	4	375.8	0.46
87.0	0.011	1.01	0.16	4	377.9	0.47
88.2	0.010	1.08	0.15	4	387.1	0.47
88.0	0.010	1.17	0.16	4	395.9	0.48
88.2	0.010	1.15	0.16	5	404.0	0.48

that MS has a predominant influence on cutting heat. Less cutting heat contributes to larger RCS. Meanwhile, larger FpT and DoC compensated for the effect of MS on the MRR. And moreover, AoU has no influence on MRR from Eq.(4). Larger amplitude should be chosen to get better RCS.

4.2.2 Multiobjective optimization II

SR is a very important index to judge the quality of finish machining, especially for precision assembly parts. Improvement of the Ra on the machined surface is an effective method, while processing efficiency also needs to be considered. Thus, the multiobjective objective II considers optimization of MRR and Ra simultaneously. The optimization model function is listed in Eq. 23.

$$\begin{cases} Object: \min f(f_4(x), f_2(x)) \\ Find: x_1, x_2, x_3, x_4, x_5 \\ s.t. \quad g_i(x) \le 0 \quad i = 1, \cdots, 10. \end{cases} \tag{23}$$

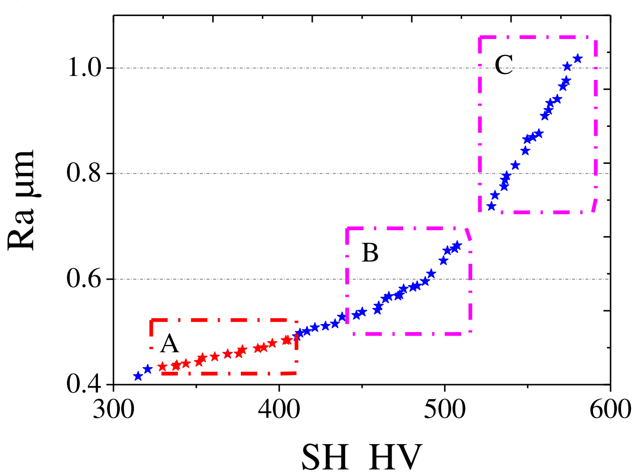

Fig. 18 Pareto front for multiobjective optimization III

After calculation, the result of optimization is drawn in Fig. 17.

From Fig. 17, it illustrates that the value of Ra increases with the increases of MRR. However, in region A, MRR increases rapidly along with a little increase of Ra. It is mean that it balances the Ra and MRR in this region. Therefore, it is regarded as an optimal region to get better Ra and higher MRR. Pareto optimal solutions of region B are listed in Table 5.

From Table 5, to balance Min (SR) and Max (MRR), smaller FpT (0.011–0.012 mm/z) and AoU (2 μm), larger MS (93.8–100 m/min), and larger DoC (0.46–0.74 mm) should be considered. The reason is that FpT and AoU have a great influence on Ra. Smaller FpT and AoU could help reduce machining residual peaks and defects and improve machining quality. Meanwhile, larger MS and DoC compensated for the effect of FpT on the MRR.

Table 7 Verification experiment design

No.	MS v, m/min	FpT f_z, mm/z	WoC a_e, mm	DoC a_p, mm	AoU A, μm
1	21.5	0.042	1.51	0.73	6
2	22.3	0.034	3.40	0.71	6
3	31.6	0.036	4.61	0.70	6
4	93.8	0.012	2.84	0.46	2
5	98.4	0.011	3.72	0.51	2
6	96.9	0.011	4.47	0.61	2
7	86.8	0.010	1.02	0.15	3
8	88.2	0.010	1.08	0.15	4
9	88.0	0.010	1.17	0.16	4

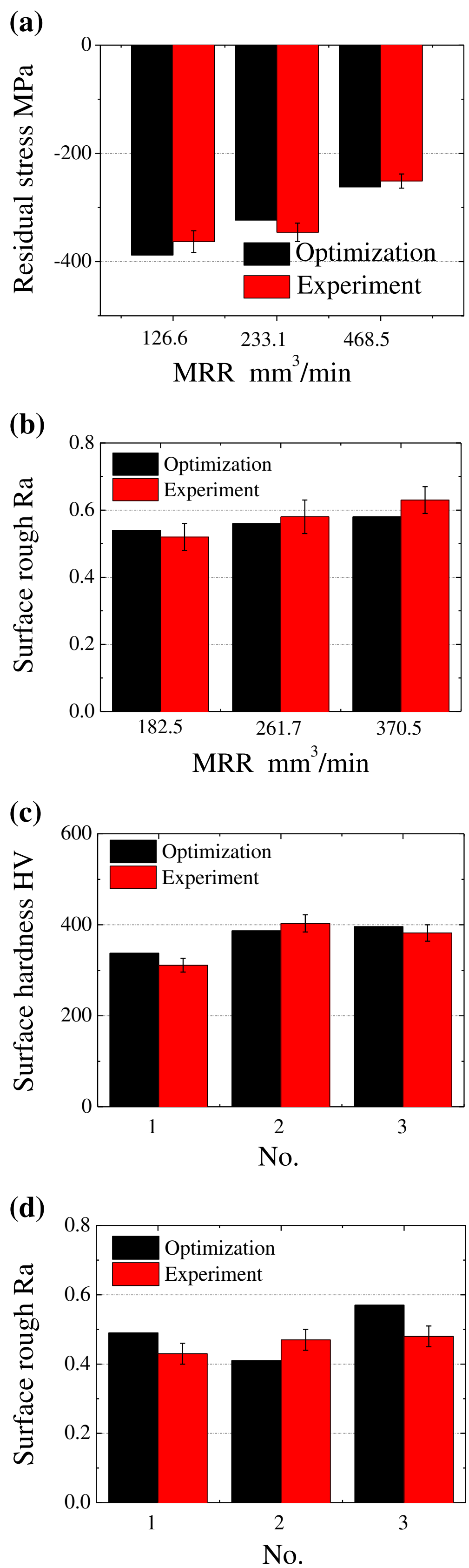

Fig. 19 **a**–**d** Verification experiment results

4.2.3 Multiobjective optimization III

Increasing the SH could increase the wear resistance of parts to a certain extent, for such parts are often used for precision assembly, and the SR of parts need be considered as well. Thus, the multiobjective objective III considers optimization of HV and Ra simultaneously. The optimization model function is given as follows:

$$\begin{cases} Object: \min f(f_2(x), f_3(x)) \\ Find: x_1, x_2, x_3, x_4, x_5 \\ \text{s.t.} \quad g_i(x) \le 0 \quad i = 1, \cdots, 10. \end{cases} \tag{24}$$

After calculation, the result of optimization is drawn in Fig. 18. It can be seen from Fig. 18. The value of Ra increases rapidly along with a litter increase of SH in regions B and C. Meanwhile, the SH increases rapidly along with a litter increase of Ra in region A. It balances the Ra and HV in this region. Therefore, it is regarded as an optimal region to get better SR and SH. Pareto optimal solutions of region A are listed in Table 6.

From Table 6, to balance Min (SR) and Max (SH), smaller FpT (0.010–0.011 mm/z) and DoC (0.15 mm), and larger MS (86.8–88.2 m/min) should be considered. Meanwhile, the appropriate WoC and AoU need to be selected according to the requirements.

5 Verification experiment for multiobjective optimization results

In order to judge the results of the multiobjective optimization, verification experiment was carried out in accordance with Table 7. It verifies multiobjective optimization I from no. 1 to 3 in Table 7, no. 4 to 7 for multiobjective optimization II, and no. 4 to 7 for multiobjective optimization III. According to the results of verification experiment and optimization, comparison results were drawn in Fig. 19, to be specific, Fig. 19a for multiobjective optimization I, Fig. 19b for multiobjective optimization II, and Fig. 19c, d for multiobjective optimization III.

It can be seen from Fig. 19 that the optimization results are close to experiment results. It proves that all the optimization models have high precision and provide choices for engineering application.

6 Conclusions

In this work, longitudinal-torsion ultrasonic vibration has been composited to the milling of titanium alloy (Ti-6Al-4V). Milling experiments have been proposed to evaluate influence of the machining and AOU parameters on machining results. To meet the different demands, three multiobjective optimization models are established to optimize milling parameters, and milling-verified experiments were carried out for optimized results. The results show that the three optimization models balance the different objective well, and the optimization results are close to experiment results. It provides choices for engineering application.

1. It is an effective method for machining of Ti-6Al-4V that longitudinal-torsion ultrasonic vibration has been superimposed to the milling, especially to obtain the surface compressive stress.
2. A multiobjective optimization model of MRR and RS has been established, to balance the processing efficiency and surface stress. A range of parameters has been obtained: MS, 21.5–37.5 m/min; FpT, 0.036–0.039 mm/z; WoC, 1.5–4.7 mm; DoC, 0.61–0.74; and AoU, 6 μm.
3. A multiobjective optimization model of MRR and Ra has been established, to balance the processing efficiency and surface quality. A range of parameters has been obtained: MS, 93.8–100 m/min; FpT, 0.011–0.012 mm/z; WoC, 2.84–4.95 mm; DoC, 0.46–0.74; and AoU, 2 μm.
4. A multiobjective optimization model of HV and Ra has been established, to balance the surface hardness and surface quality. A range of parameters has been obtained: MS, 86.8–88.3 m/min; FpT, 0.010–0.011 mm/z; WoC, 1.02–1.17 mm; DoC, 0.15–0.16; and AoU, 2–5 μm.

Acknowledgements The paper is sponsored by the National Natural Science Foundation of China (No. 51475148) and Henan Research Program of Fundamental and Frontier Technology (No. 152300410102).

References

1. Oh JM, Heo KH, Kim WB, Choi GS, Lim JW (2013) Sintering properties of Ti-6Al-4V alloys prepared using Ti/TiH2 powders. Mater Trans 54:119–121. doi:10.2320/matertrans.M2012304
2. Ellyson B, Brochu M, Brochu M (2017) Characterization of bending vibration fatigue of SLM fabricated Ti-6Al-4V. Int J Fatigue 99: 25–34. doi:10.1016/j.ijfatigue.2017.02.005
3. Mohsan AUH, Liu Z, Padhy GK (2017) A review on the progress towards improvement in surface integrity of Inconel 718 under high pressure and flood cooling conditions. Int J Adv Manuf Technol 91: 107–125. doi:10.1007/s00170-016-9737-3
4. Shokrani A, Dhokia V, Newman ST (2016) Investigation of the effects of cryogenic machining on surface integrity in CNC end milling of Ti-6Al-4V titanium alloy. J Manuf Process 21:172–179. doi:10.1016/j.jmapro.2015.12.002
5. Jackson MJ, Novakov T, Da Silva MB, Machado AR (2017) Predicting chip and non-chip formation when micromachining Ti-6Al-4V titanium alloy. Int J Adv Manuf Technol 91:955–985. doi: 10.1007/s00170-016-9754-2
6. Grigoriev SN, Vereschaka AA, Fyodorov SV, Sitnikov NN, Batako AD (2017) Comparative analysis of cutting properties and nature of wear of carbide cutting tools with multi-layered nano-structured and gradient coatings produced by using of various deposition methods. Int J Adv Manuf Technol 90:3421–3435. doi:10.1007/s00170-016-9676-z
7. Jiao F, Niu Y, Liu X (2015) Effect of ultrasonic vibration on surface white layer in ultrasonic aided turning of hardened GCr15 bearing steel. Mater Res Innov 19:938–942. doi:10.1179/1432891715Z.0000000001844
8. Tao G, Ma C, Shen X, Zhang J (2017) Experimental and modeling study on cutting forces of feed direction ultrasonic vibration-assisted milling. Int J Adv Manuf Technol 90:709–715. doi:10.1007/s00170-016-9421-7
9. Ko JH, Ehmann KF (2013) Investigation of the effect of tooling axial ultrasonic vibration assistance on meso-scale milled surfaces, Berlin, Germany, [C]. euspen, 2013
10. Ahmed Y, Cong WL, Stanco MR, Xu ZG, Pei ZJ, Treadwell C, Zhu YL, et al. (2012) Rotary ultrasonic machining of alumina dental ceramics: a preliminary experimental study on surface and subsurface damages. J Manuf Sci Eng, Trans ASME, 134 doi: 10.1115/1.4007711
11. Hara K, Isobe H, Ismail MF (2012) Ultrasonically assisted machining for mirror finishing of die (3rd report)—a research of effects of cutting edge truncation on grinding phenomenon. Seimitsu Kogaku Kaishi/Journal of the Japan Society for Precision Engineering 78:641–645
12. Wang M, Li S, Zheng Y (2014) Surface roughness of titanium alloy under ultrasonic vibration milling. Nongye Jixie Xuebao/Trans Chin Soc Agric Mach 45:341–346. doi:10.6041/j.issn.1000-1298.2014.06.052
13. Jiang X, Liang H, Lu H, Dai J, Zhang D (2014) Investigation of ultrasonic elliptical vibration milling of thin-walled titanium alloy parts. Binggong Xuebao/Acta Armamentarii 35:1891–1897. doi: 10.3969/j.issn.1000-1093.2014.11.022
14. Soutome T, Sato K (2013) Study on ultrasonic vibration cutting (2nd report)—analysis and consideration of cylindrical profile and surface roughness by vibration cutting on thrust force direction. Seimitsu Kogaku Kaishi/J Jpn Soc Precis Eng 79:766–772
15. Budak E, Altintas Y (1992) Flexible milling force model for improved surface error predictions, Istanbul, Turk, 1992[C]. Publ by ASME
16. Merdol SD, Altintas Y (2008) Virtual simulation and optimization of milling operations—part I: process simulation. J Manuf Sci Eng Trans ASME 130:510041–5100412. doi:10.1115/1.2927434
17. Liu C, Tang D, He H, Chen X (2013) Prediction of surface roughness for end milling titanium alloy using modified particle swarm optimization LS-SVM. Trans Nanjing Univ Aeronaut Astronaut 30:53–61
18. Mahdavinejad RA, Khani N, Fakhrabadi MMS (2012) Optimization of milling parameters using artificial neural network and artificial immune system. J Mech Sci Technol 26:4097–4104. doi:10.1007/s12206-012-0882-9
19. Brecher C, Fey M, Tenbrock C, Daniels M. (2016) Multipoint constraints for modeling of machine tool dynamics. J Manuf Sci Eng Trans ASME,138. doi: 10.1115/1.4031771
20. Li J, Yang X, Ren C, Chen G, Wang Y (2014) Multiobjective optimization of cutting parameters in Ti-6Al-4V milling process using nondominated sorting genetic algorithm-II. Int J Adv Manuf Technol 76:941–953. doi:10.1007/s00170-014-6311-8
21. Chakraborti N, Siva Kumar B, Satish Babu V, Moitra S, Mukhopadhyay A (2006) Optimizing surface profiles during hot rolling: a genetic algorithms based multi-objective optimization. Comput Mater Sci 37:159–165. doi:10.1016/j.commatsci.2005.12.031
22. Koura OM, El-Akkad AS (2016) Optimization of cutting conditions using regression and genetic algorithm in end milling. Int J Eng Res Afr 20:12–18. doi:10.4028/www.scientific.net/JERA.20.12
23. Gholami MH, Azizi MR (2014) Constrained grinding optimization for time, cost, and surface roughness using NSGA-II. Int J Adv Manuf Technol 73:981–988. doi:10.1007/s00170-014-5884-6
24. Emmanuel Nicholas P, Lenin Babu MC, Sathya SA (2016) Multiobjective optimization of laminated composite plate with elliptical cut-out using ANN based NSGA-II. J Mech Mater Struct 11:157–172. doi:10.2140/jomms.2016.11.157
25. Deb K, Datta R (2012) Hybrid evolutionary multi-objective optimization and analysis of machining operations. Eng Optim 44:685–706. doi:10.1080/0305215X.2011.604316